Atom trapping and two-dimensional Bose-Einstein condensates in field-induced adiabatic potentials

O. Zobay
Theoretische Quantenphysik, Technische Universität Darmstadt, Hochschulstrasse 4a, 64289 Darmstadt, Germany

B. M. Garraway
Department of Physics and Astronomy, University of Sussex, Brighton BN1 9QH, United Kingdom
(Received 6 June 2003; published 6 February 2004)

We discuss a method to create two-dimensional (2D) traps as well as atomic shell, or bubble, states for a Bose-Einstein condensate initially prepared in a conventional magnetic trap. The scheme relies on the use of time-dependent, radio-frequency-induced adiabatic potentials. These are shown to form a versatile and robust tool to generate interesting trapping potentials. Our shell states take the form of thin, highly stable matter-wave bubbles and can serve as stepping stones to prepare atoms in highly excited trap eigenstates or to study ''collapse and revival phenomena.'' Their creation requires gravitational effects to be compensated by applying additional optical dipole potentials. However, in our scheme gravitation can also be exploited to provide a route to two-dimensional atom trapping. We demonstrate the loading process for such a trap and examine experimental conditions under which a 2D condensate may be prepared.

DOI: 10.1103/PhysRevA.69.023605 PACS number(s): 03.75.Be, 42.50.Vk, 32.80.Pj, 03.75.Mn

I. INTRODUCTION

Due to the rapid advances in experimental and theoretical atom optics, it has now become possible to cool atoms down to extremely low temperatures. An important characteristic of such ultracold atoms is their sensitivity to very weak external potentials. In the context of atomic Bose-Einstein condensation, this feature is particularly attractive. The condensate can be described, to a very good degree of approximation, in terms of a single macroscopic wave function which in this way can be subjected to intricate probing and manipulation. Consequently, in recent years various ingenious techniques for handling Bose-Einstein condensates (BECs) have been developed that exploit this sensitivity, e.g., magnetic quadrupole and time-orbiting potential (TOP) traps, shallow optical dipole traps, phase-imprinting methods to create solitons or vortices, and radio-frequency (rf) output coupling, to name but a few prominent examples (for a review of these and other techniques, see Ref. [1]). However, the development of further tools and methods still presents a significant objective of current work, and forms the basis for advancing research in several main areas of BEC physics.

One such area concerns the experimental realization of low-dimensional Bose-Einstein condensates of trapped dilute atomic gases. Under reduced dimensionality, the condensate properties differ drastically from the well-studied three-dimensional case and have been under intense theoretical debate for some time [2,3]. Low-dimensional BECs are characterized by the fact that due to strong confinement by the external trapping potential one or more motional degrees of freedom become quantum-mechanically frozen before the condensation point is reached. Major obstacles, that had been confronting the preparation of one- or two-dimensional (2D) BECs for a long time, concerned the construction of suitable traps—e.g., very high field gradients would be required for magnetic traps—as well as the development of efficient loading procedures. Only recently has it become possible to overcome these difficulties, and the first realizations of atomic BECs in two dimensions have been reported [4–6]. In these experiments, the dimensionality is reduced by exposing the atoms to steep optical potentials. In Ref. [4], single one- or two-dimensional BECs are prepared, whereas in the experiments of Refs. [5,6] the use of optical lattices led to the creation of arrays of two-dimensional condensates. However, in addition to these works, various other interesting ideas regarding the manufacture of two-dimensional traps have been put forward over the last few years. In these proposals, trapping is provided either by optical [7] or by magnetic [8] means, whereas loading is accomplished through optical pumping.

The purpose of the present paper is twofold. On the one hand we wish to promote field-induced adiabatic potentials as a versatile tool to manipulate ultracold atoms and, in particular, Bose-Einstein condensates. On the other hand, we show that they offer a route to the creation of two-dimensional traps for BECs. An initial outline of our results was given in Ref. [9]. Adiabatic potentials arise whenever two or more internal atomic states, that experience different potentials for the atomic center-of-mass motion, are coupled by a strong resonant external field. The atomic motion is then no longer dominated by the different ''bare'' potentials but is usefully described in terms of the adiabatic potentials that arise from the diagonalization of the bare potentials and the couplings at each spatial point. Adiabatic potentials have been in use for some time as the underlying mechanism for evaporative cooling. However, to our knowledge, little attention has been paid to the fact that they offer a lot of further possibilities to control quantum-mechanical atomic motion (one fairly recent application is described in Ref. [10]). In this paper we will give some examples of the application of adiabatic potentials as a tool for manipulating matter waves, and we hope to stimulate further research in this direction.

After giving a qualitative introduction to adiabatic potentials in Sec. II, we continue in Sec. III to show how they can

be employed to create so-called ''matter-wave bubbles'' from a BEC initially trapped in the ground state of a harmonic potential. In the bubble state the wave function is localized around the surface of a sphere so that the matter density forms a spherical shell or bubble. We give a detailed account of the preparation of bubble states and their decay rates induced by nonadiabatic leakage. In particular, we address the question of how to compensate for gravitational effects in the laboratory which otherwise would impede the creation process. We expect matter-wave bubbles to have interesting applications, some of which are investigated in Sec. IV. There it is shown that they can be used as stepping stones to prepare atoms in highly excited eigenstates of the bare harmonic trapping potential and to create new types of nonlinear eigenstates of BECs. Furthermore, we examine collapse and revival effects which are found when the external coupling is switched off. By also switching off the trapping potential we can observe the free bubble expansion.

In Sec. V we turn to the investigation of gravitational influences on the bubble preparation process. At first sight gravity is seen to be detrimental, but it is shown that it can be exploited to obtain a scheme for the creation of two-dimensional BECs. Gravity will cause the atoms in the shell potential to pool at the bottom of the trap so that the condensate forms a flat disk. In Sec. V the initial transfer of a BEC into such a disk state in the course of switching on the external field is examined numerically. In particular, we show that if the field parameters are changed appropriately the disk radius is steadily increased whereas its width keeps shrinking due to enhanced confinement. This suggests that the continuation of this process could ultimately yield a two-dimensional trap for the BEC, although the numerical study of the approach to this limit is not currently feasible. In Sec. VI we further pursue this idea by giving some general qualitative, and semiquantitative, estimates and arguments about the conditions necessary to reach the 2D regime. They indicate the feasibility of our approach by showing that the requirements for the applied fields, preservation time of the condensate, etc. are demanding but still within the reach of currently available technology. The paper ends with brief conclusions and outlook given in Sec. VII.

The most important difference to the previous proposals of Refs. [7,8] for creating 2D traps is the fact that our method relies on adiabatically deforming a conventional magnetic trap and does not require incoherent processes, e.g., optical pumping, for loading. This would allow for working with extremely cold, dense, and, possibly, coherent atomic ensembles throughout the whole process. In comparison to the experiments [4–6], our scheme does not make use of optical potentials, but a combination of magnetic and rf fields. It thus avoids potential difficulties with spontaneous emission in very steep optical traps that require high laser intensities. In contrast to Refs. [5,6], our proposal produces a single condensate with a large number of atoms, similar to the experiment of Ref. [4]. However, the trapping frequencies obtainable in the rf scheme might be significantly higher trapping frequencies than the ones reported in the latter work.

II. ADIABATIC POTENTIALS

The basic principles of adiabatic potentials can be understood from examining a quantum-mechanical two-state particle that propagates in the vicinity of a linear potential crossing. In the interaction picture, with respect to the coupling field that gives rise to the crossing, the Schrödinger equation for this system is written as follows:

$$i\dot{\phi}_1=\left(-\frac{1}{2}\frac{\partial^2}{\partial r^2}+Cr\right)\phi_1+\Omega\phi_2,$$

$$i\dot{\phi}_2=\left(-\frac{1}{2}\frac{\partial^2}{\partial r^2}-Cr\right)\phi_2+\Omega\phi_1. \tag{1}$$

We can transform this equation to a basis that diagonalizes the potentials $\pm Cr$ and the coupling Ω at each point, i.e., to the basis of the spatially dependent ''dressed eigenstates.'' In this basis the Schrödinger equation has the form [11]

$$i\dot{\phi}_+=\left[-\frac{1}{2}\frac{\partial^2}{\partial r^2}+V_+(r)+V_{kin}(r)\right]\phi_++V_c(r,\partial_r)\phi_-,$$

$$i\dot{\phi}_-=\left[-\frac{1}{2}\frac{\partial^2}{\partial r^2}+V_-(r)+V_{kin}(r)\right]\phi_--V_c(r,\partial_r)\phi_+. \tag{2}$$

The potentials $V_\pm(r)$ are the adiabatic potentials and are given by

$$V_\pm(r,t)=\pm\sqrt{(Cr)^2+\Omega^2}. \tag{3}$$

They arise from the pointwise diagonalization of the 2×2 matrix formed by $\pm Cr$ and Ω. The terms

$$V_{kin}(r)=\frac{C^2}{8\Omega^2[1+(Cr/\Omega)^2]^2} \tag{4}$$

and

$$V_c(r,\partial_r)=\frac{C}{2\Omega[1+(Cr/\Omega)^2]}\left[\frac{C^2r}{\Omega^2[1+(Cr/\Omega)^2]}-\frac{\partial}{\partial r}\right] \tag{5}$$

stem from the nonlocal character of the kinetic-energy term.

We see that $V_+(r)+V_{kin}(r)$ is a binding potential. If the coupling term $V_c(r,\partial_r)$ were not present, a wave packet prepared in the state ''+'' would remain trapped forever in the potential $V_+(r)+V_{kin}(r)$. However, if Ω is small the coupling V_c is dominant. In this case any wave packet quickly leaves the crossing region around $r\simeq0$, and the description given by Eq. (2) is not useful. Nevertheless, if Ω is increased, the kinetic coupling V_c (as well as V_{kin}) rapidly becomes small [12] and the motion of the wave packet is more and more determined by the adiabatic potentials $V_\pm$. In fact, it is shown in Sec. III B that the lifetime of a wave packet prepared in the internal state +, i.e., the time it takes

the wave packet to transfer to the state "$-$" and leave the crossing region, increases exponentially with Ω.

At first sight, it seems counterintuitive that it is possible to trap a particle, even with strong coupling, between two potentials in a region where the particle is not stable. We can draw an analogy with a particle moving in a magnetic quadrupole field. Each of its bare Zeeman substates (with "bare" meaning having fixed spatial orientation) individually would experience the field as unstable. However, if the particle moves slowly enough, couplings between the states are induced so that the particle's orientation with respect to the local direction of the total magnetic field is preserved. In this way, trapping can ensue for weak-field seeking states. In the case considered here, a slow particle tends to remain in the same dressed eigenstate and its motion is governed by the adiabatic potentials.

III. CREATION OF MATTER-WAVE BUBBLES

A. Basic approach

To work out the basic ideas of our approach we first discuss its realization in the absence of gravity. As a result, we obtain a scheme to produce thin, highly stable matter-wave bubbles or shells in which the trapped atoms are localized around the surface of a sphere.

The starting point for our method is a coherent sample of atoms produced, e.g., by Bose-Einstein condensation and trapped in the ground state of a harmonic magnetic potential. The preparation scheme then proceeds by applying a sequence of radio-frequency fields that couple the initial internal atomic state, a weak-field seeking Zeeman sublevel, to a second hyperfine ground state (multilevel excitation schemes can be considered as well, see Sec. V). As mentioned above, the preparation process may appear to be counterintuitive as the second state is an untrapped, high-field seeking state [see inset, Fig. 1(a)]. As this technique also forms the basis of evaporative cooling, one may be led to expect that this procedure will inevitably cause a rapid depletion of the trapped atomic population. Nevertheless, as was anticipated in Sec. II and is also shown below, if the fields are controlled in an appropriate way one may also obtain a very different effect.

To model the creation of our bubble states we study the coherent time evolution of a condensate initially prepared in a hyperfine state $|1\rangle$ in the ground state of a spherically symmetric magnetic trap. When $t>0$ external fields are applied that induce a coupling of state $|1\rangle$ to a Zeeman sublevel $|2\rangle$ whose magnetic moment is supposed to be equal in magnitude but opposite in sign. Such a coupling may be realized, e.g., as a transition between the hyperfine ground states $|F=1,m_F=-1\rangle$ and $|F=2,m_F=-1\rangle$ in ^{87}Rb [13]. The field-induced coupling strength is denoted as Ω and is spatially independent to a good degree of approximation. In the following model we assume a radial $l=0$ form of the wave-function components $\psi_i(\mathbf{r})=\phi_i(r)/\sqrt{4\pi}r$. Then working in an interaction picture with respect to the applied fields, the time development is determined by the radial Gross-Pitaevskii equation

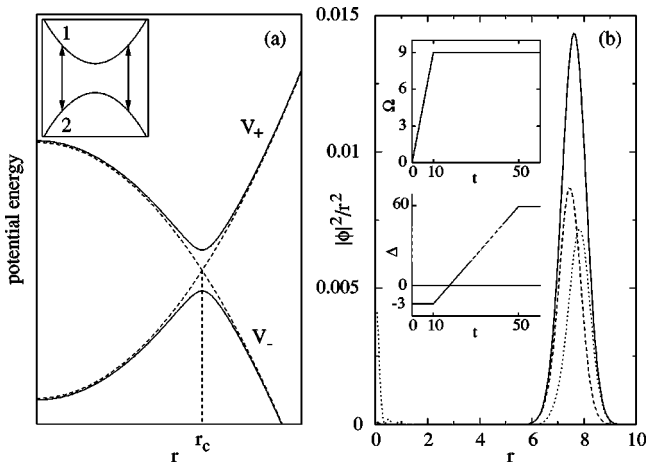

FIG. 1. (a) Schematic of field-induced adiabatic potentials $V_\pm$ for $\Delta>0$. Dashed curves show the bare potentials crossing at r_c. Inset: bare potentials showing resonance at r_c. (b) Bubble, or shell, state as obtained by the preparation scheme discussed in the text with (in scaled units) $\Delta_{final}=60.0$ and $\Omega_{final}=9.0$ (see inset). Full curve: atomic density $|\phi_+|^2/r^2$ in the adiabatic state $+$; dotted and dashed curves show $|\phi_1|^2/r^2$ and $|\phi_2|^2/r^2$, respectively. Nonlinear effects are not included here.

$$i\dot{\phi}_1=\left(-\frac{1}{2}\frac{\partial^2}{\partial r^2}+\frac{r^2}{2}-\frac{\Delta(t)}{2}\right)\phi_1+\Omega(t)\phi_2$$
$$+N(U_{11}|\phi_1|^2+U_{12}|\phi_2|^2)\frac{\phi_1}{r^2},$$
$$i\dot{\phi}_2=\left(-\frac{1}{2}\frac{\partial^2}{\partial r^2}-\frac{r^2}{2}+\frac{\Delta(t)}{2}\right)\phi_2+\Omega(t)\phi_1$$
$$+N(U_{12}|\phi_1|^2+U_{22}|\phi_2|^2)\frac{\phi_2}{r^2}. \quad (6)$$

In this equation time is scaled to the trap inverse oscillator frequency ω^{-1}, length is scaled to the harmonic-oscillator length scale a_{ho}, and $\Omega(t)$ and $\Delta(t)$ are scaled to $\hbar\omega$. The effective detuning is defined by $\Delta(t)=[\hbar\omega_f-\Delta E(0)]/\hbar\omega$, where $\Delta E(0)$ is the energy difference between the two hyperfine states at the origin (trap center) and ω_f the frequency of the applied field. The nonlinearity parameters are given by $U_{ij}=a_{ij}/a_{ho}$ with a_{ij} the scattering lengths for intraspecies and interspecies collisions. The states are normalized according to $\int_0^\infty dr(|\phi_1|^2+|\phi_2|^2)=1$. The total number of atoms is denoted N.

The strategy that we pursue in our engineering scheme is to control the condensate by slowly changing field-induced adiabatic (or dressed) potentials. These potentials, which are defined as the spatially dependent eigenvalues of the potentials and couplings in Eqs. (6), are given by [cf. Eq. (3)]

$$V_\pm(r,t)=\pm\sqrt{[r^2-\Delta(t)]^2/4+\Omega^2(t)} \quad (7)$$

and are depicted for $\Delta>0$ in Fig. 1(a). The potential V_- actually gives rise to the evaporative cooling effect in the

usual arrangement. In that case one applies a field with an effective detuning which is large compared to the mean particle energy. The atoms then move in the potential V_-, and the ones that reach its maximum, from the left, with sufficiently slow velocity, go over the top and get expelled from the trap. However, we will show that the atoms can also be prepared in the lowest-energy eigenstate (or, more exactly, resonance) $|0\rangle \equiv |0;\Omega,\Delta\rangle$ of the potential V_+. This quasibound or ''trapping'' state $|0\rangle$ will realize the spherical shell state or matter-wave bubble [see Fig. 1(b) and Ref. [14]]. The state will be localized around the crossing of the two bare potentials at $r_c=\sqrt{\Delta}$ and have a width of $\Delta r = (\Omega/\Delta)^{1/4}$, provided a harmonic expansion around the potential minimum is justified. The state is a genuine superposition of the internal states $|1\rangle$ and $|2\rangle$.

B. Lifetime of bubbles

Before considering the bubble preparation process in detail one question immediately arises, i.e., the stability of the system once it is prepared in the state $|0\rangle$. At first it is not obvious that atoms may remain trapped for a substantial time at the point of maximum effective coupling between states $|1\rangle$ and $|2\rangle$. As we have discussed in Sec. II, it becomes more plausible if one transforms Eqs. (6) to the dressed-state basis, i.e., the basis that diagonalizes the bare potentials and the coupling at each point r. In this picture the two wave-function components appear coupled by kinetic terms whose significance is rapidly diminished when Ω is increased. If nonlinear interactions can be neglected, the decay rate γ of the trapping state $|0\rangle$ can be determined with the help of semiclassical methods developed in connection with molecular predissociation [15,16]. As we show in the Appendix, from these techniques it follows that $\gamma=-2\,\mathrm{Im}\,E_0$, where the complex ground-state energy E_0 is determined as a solution of

$$[e^{2\pi\delta(E)}-1]\cos\Phi(E)e^{-i[\beta(E)-\Phi(E)]}+\cos\beta(E)=0 \quad (8)$$

with $\beta(E)=\pi(2E+\Delta-1)/4$ and the parameters $\delta(E)$ and $\Phi(E)$ characterizing the scattering matrix of the linearized potential crossing problem. For these quantities there are several analytical approximations in the literature [17]; following, e.g., Ref. [15] one can put $\delta(E)=1/8ab$ and $\Phi(E) = 2b^3/3a+\arg\Gamma[i\delta(E)]+\delta(E)\ln[\delta(E)]-2\delta(E)\ln(b/a)+\pi/4$ with $a^2=\Delta/(8\Omega^3)$ and $b^2=E/\Omega$. For large enough Ω one obtains

$$\gamma=\frac{2\cos^2\beta(E)}{\{\exp[2\pi\delta(E)]-1\}(\partial\Phi/\partial E)}, \quad (9)$$

where all quantities have to be evaluated at $\mathrm{Re}\,E_0\simeq\Omega+\sqrt{\Delta/4\Omega}$. The comparison in Fig. 2(a) between the predictions of Eqs. (8) and (9) and the direct numerical determination of decay rates from Eqs. (6) indicates the validity of these approximations. To obtain the numerical decay rates we first generated the bubble state at a required (Δ,Ω) by performing the preparation process (which will be described in detail in Sec. III C). We then monitored the decay of the norm of the wave function in the internal state + as a function of time. After an initial transient, this decay was exponential to a very good degree of approximation.

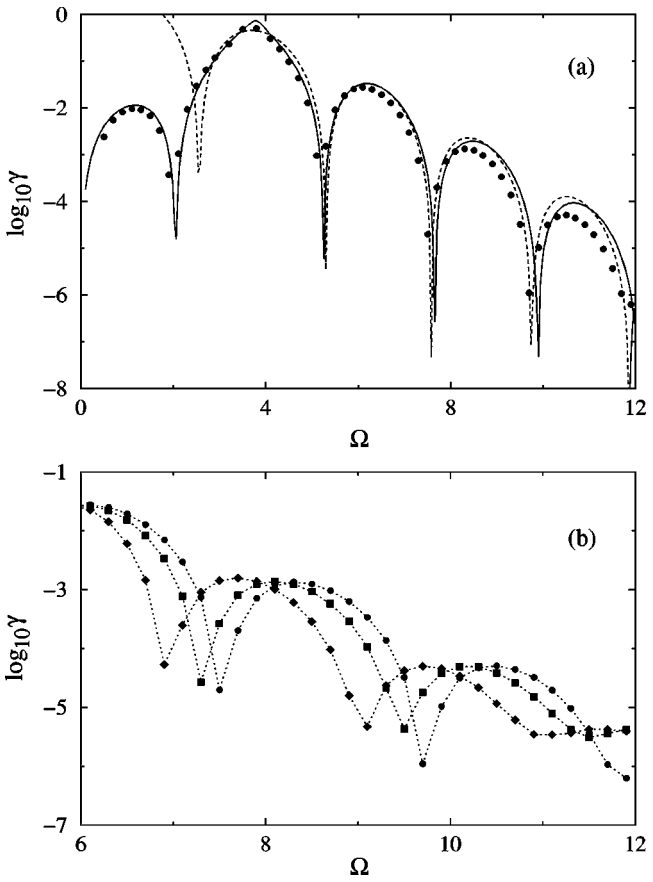

FIG. 2. (a) Evaluation of decay rates $\gamma(\Omega)$ for bubble states (without atomic interactions) according to Eqs. (8) (full curve) and (9) (dashed) at $\Delta=61.0$, using the approximations of Ref. [15]. Circles: numerical values determined from Eq. (6). (b) Influence of atomic interactions on decay rates. Numerical calculation of $\gamma(\Omega)$ according to Sec. III C for $UN=0$ (full circles), 33 (open squares), and 99 (full diamonds). Dotted lines are to guide the eye. Note the different ranges of abscissa values in (a) and (b).

Equation (9) yields two important insights: first, the decay is exponentially suppressed with growing Ω. In the limit of $\gamma \ll 1$, this exponential suppression may be approximated as

$$\gamma_{ex}\sim 2\exp(-\pi\Omega^{3/2}/\sqrt{2}\Delta^{1/2}). \quad (10)$$

Second, for $\mathrm{Re}E_0=2k+3/2-\Delta/2$, with integer k, the decay rates become very small. In these cases the state $|0\rangle$ is in resonance with an eigenstate of the bare harmonic trapping potential. This stabilization effect may be used to obtain extremely long-lived states already for moderate coupling strengths.

C. Preparation

Having established the existence of long-lived spherical bubble states in adiabatic potentials, we now turn to the details of their preparation. The first phase is to let the bare harmonic potential of state 1 evolve smoothly into the dressed potential V_+ and the second phase is to expand the

bubble outwards. Both phases are done so that the wave function is kept at all times in the instantaneous ground state $|0;\Omega(t),\Delta(t)\rangle$. In the example of Fig. 1(b) (in which nonlinear effects have been neglected) we achieve the first phase by increasing Ω to the final (scaled) value of 9 at fixed *negative* detuning $\Delta=-3$ [see Fig. 1(b), inset]. Then the second phase of bubble expansion is achieved by maintaining the intensity, but gradually ramping up the detuning. In this way less than 4% of the initial population was lost before reaching the final state shown in Fig. 1(b). The particular merit of this approach is that there is no need to follow a precisely prescribed path as the method relies on adiabatic following [in a similar way to the wave packet guidance in adiabatic passage by light induced potentials (APLIP) [18]]. Any field sequence that guides the system sufficiently slowly through states of long lifetime is suitable.

If we make our atomic bubbles from an initial BEC, we should also study the effects of the nonlinear interactions introduced in Eq. (6). The dressed-state description is readily generalized if $U_{11}\simeq U_{22}\simeq U_{12}=U$ (such a situation is realized, e.g., in the Na $F=1$ hyperfine multiplet [1]). Under these circumstances we can still define an adiabatic wave function ϕ_+ that evolves, to a good degree of approximation, according to the Gross-Pitaevskii equation

$$i\dot{\phi}_+=\left[-\frac{1}{2}\frac{\partial^2}{\partial r^2}+V_+(r,t)+NU\frac{|\phi_+|^2}{r^2}\right]\phi_+. \qquad (11)$$

In particular, for a sufficiently strong nonlinearity U, the atomic density can be described by the Thomas-Fermi ansatz

$$|\phi_+|^2=[\mu-V_+(r,t)]/NU \qquad (12)$$

with the chemical potential μ determined by the normalization condition. Numerical studies show that shell, or bubble, states can then be manufactured in the same way as before. Figure 2(b) demonstrates that the atomic interactions affect the lifetimes of the shell states only slightly. In this diagram, instantaneous decay rates γ for nonlinear interactions $NU=0$, 33, and 99 are shown as a function of Ω at the same detuning $\Delta=61$ as in Fig. 2(a). (For ^{87}Rb, these values of NU correspond to 20 000 and 60 000 atoms, respectively.) The plot focusses on the regime of larger Ω, where the average lifetime clearly displays the exponential dependence on the coupling strength. The decay rates have been determined in the same way as for the linear system; it had to be ensured, however, that the numerical ''observation times'' were chosen sufficiently short so that the shell state population decreases only slightly. Over these short periods, the decay is still exponential. As soon as the population is diminished appreciably, it is apparent from Fig. 2(b) that the decay rates change thus leading on the whole to a nonexponential decay process. Figure 2(b) indicates that, at least for the examined range of values, the atomic interactions do not modify the behavior of the decay rates profoundly; their main influence is a change in the position of the ''resonances'' where the lifetime becomes extremely large. We mostly attribute this effect to a modification of the resonance conditions due to the mean-field shifts $\Delta\mu$ resulting from the atomic interactions.

In the discussion of the bubble preparation we have so far assumed that the atomic self-interaction and cross interaction are approximately equal. If they differ significantly, however, numerical simulations indicate that the creation of bubble states becomes more difficult and their lifetime is reduced.

D. Bubbles with gravitational field compensation

So far, we have neglected the influence of gravity. Its effect on the bubbles is expected to be detrimental as it will cause the atoms to pool at the bottom of the shell potential. In this section, we first give a simple estimate of how strong the gravitational influence must be to cause significant deviations from a homogeneous density distribution in the bubble state. We then propose a method to compensate for gravitation in the laboratory with the help of optical potentials.

When the bubble width is small compared to the radius, the radial dependence of the adiabatic potential is approximately harmonic with a minimum at the bubble radius $r_0=\sqrt{\Delta}$ and an anguar frequency $\omega_0=\sqrt{\Delta/\Omega}$ [14]. Thus, we can approximate the Hamiltonian for atoms in the trapping internal state + as

$$H=-\frac{\nabla^2}{2}+\frac{1}{2}\omega_0(r-r_0)^2+Gr\cos\theta, \qquad (13)$$

with the radial and polar coordinates r,θ, and the scaled gravitational acceleration $G=g\sqrt{m/\hbar\omega_z^3}$ (with $g\simeq 9.81\ \mathrm{ms}^{-2}$). We now make the ansatz

$$\psi_{tr}(r,\theta)=\frac{1}{\sqrt{\mathcal{N}}}\frac{\exp[-(r-r_0)^2/2\sigma^2]}{r}f(\cos\theta) \qquad (14)$$

for the ground state of this Hamiltonian, where $\sigma=1/\sqrt{\omega_0}$. This ansatz implies that, radially, the wave function is always in the ground state, i.e., the influence of gravity is manifest only in the polar envelope $f(\cos\theta)$. For present purposes it is sufficient to choose a very simple form for f, e.g., $f(\cos\theta)=a\cos\theta+b$. The normalization factor in Eq. (14) is then given by $\mathcal{N}=\sqrt{\pi}(2a^2/3+b^2)/\sigma$. Furthermore, a variational calculation shows that a and b are related by $a/b=Q-\sqrt{Q^2+3/2}$ with $Q=3/4Gr_0^3$. A significant influence of gravity is certainly present when $f(\cos 0)=0$, i.e., $a/b=-1$, as in this case the bubble has ''opened up.'' This is realized for $Q\simeq 0.17$ or, in unscaled coordinates,

$$r_0\simeq(3\hbar^2/gm^2)^{1/3} \qquad (15)$$

which is about 5.5×10^{-7} m for ^{87}Rb. In the presence of gravity, bubbles can therefore only be observed in spherical traps with trapping frequencies large compared to 400 Hz. The estimate (15) can be interpreted as a balance condition between kinetic and gravitational energy which are of the order $\hbar^2/2mr_0^2$ and mgr_0, respectively.

The detrimental influence of gravity can, at least in principle, be compensated for by exposing the trapped atoms to an additional optical dipole potential. In a typical Gaussian beam configuration this potential, which acts on all hyperfine sublevels in the same way, is given by [1]

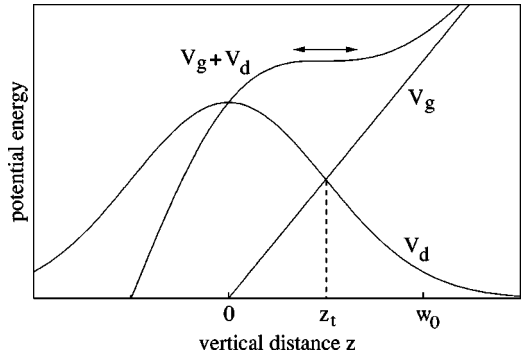

FIG. 3. Schematic showing the local compensation of gravity with the help of an optical potential. Shown are dipole potential V_d, the gravitational potential V_g, and their sum. The arrow indicates the flat region of the combined potential in which a bubble might be created.

$$V_d(x,\varrho)=\frac{V_0}{1+(x/x_R)^2}\exp\left\{-\frac{2\varrho^2}{w_0^2[1+(x/x_R)^2]}\right\} \quad (16)$$

with $\varrho=\sqrt{y^2+z^2}$. The Rayleigh length x_R and the beam waist radius w_0 are related by $x_R=\pi w_0^2/\lambda_{op}$ with λ_{op} the wavelength of the optical field. Finally, in unscaled units, $V_0=3\Gamma c^2P/\Delta w_0^2\omega_0^3$, where ω_0 denotes the resonance frequency, Γ the spontaneous decay rate of the excited state, Δ the detuning between laser and the atomic transition, and P the applied laser power. The idea is now to adjust the trap depth V_0 such that at the turning point z_t of the optical potential along the line $x=y=0$, which is defined by $\partial^2V_d(z_t)/\partial z^2=0$, the slope $\partial V_d(z_t)/\partial z=-mg$. In this way, the combined optical and gravitational potential is almost constant around z_t, the lowest-order corrections being cubic in $z-z_t$ (see Fig. 3). The magnetic trap has then to be placed inside this area. From Eq. (16) it follows that, as $z_t=w_0/2$, we have to choose $V_0=\exp(1/2)w_0mg/2$ to fulfil the above condition. If the condensate is in the Thomas-Fermi regime, the z extension of the volume within which a bubble could be created is somewhat less than $(w_0^2\mu/mg)^{1/3}$ with μ the BEC chemical potential [for which an estimate is given in the following section in Eq. (20)]. This follows from stipulating that the variation of the combined optical and gravitational potential over this volume should be less than μ.

We have performed numerical simulations to demonstrate that this approach actually offers the possibility to overcome the influence of gravity. To this end, we have studied the full preparation process, not with the approximate Hamiltonian (13), but using a more realistic model that will be discussed further in Sec. V A. Our simulations involve the time-dependent solution of the two-dimensional Gross-Pitaevskii equation with gravity, the optical potential, and the relevant adiabatic surface in the ^{87}Rb $F=2$ multiplet [19]. As an example we have shown that in an anisotropic trap with $\nu_z=\omega_z/2\pi=220$ Hz, $\nu_x=30$ Hz, bubble states for a BEC corresponding to an atom number of 10^5 in three dimensions can be produced at $\Delta=6.6$ kHz, $\Omega=2.6$ kHz, $V_0=-129$ kHz, and $w_0=73$ μm. For the preparation, Ω is switched on within $\Delta t=29$ ms at $\Delta=-1.1$ kHz, and then Δ is increased to its final value within $\Delta t=200$ ms. The bubble has radial and axial diameters of 15 μm and 110 μm, respectively. The necessary laser power is estimated at around 1 W. The large axial extension shows that in this direction the variation of the combined optical and gravitational potential is almost negligible. To find an optimized shape for given Ω and Δ, it is advisable to experiment by slightly varying the laser power and the position of the magnetic trap center. Nevertheless, the preparation scheme is robust in the sense that (for the configuration described above) one still obtains a bubble if the location of the magnetic trap (in z) relative to the dipole potential is changed by about $\pm10\%$, and the laser intensity by about $\pm2.5\%$. However, *during* preparation these parameters have to be stabilized very well (to within a fraction of the indicated range) to avoid excitation of the bubble.

E. Bubbles and trap anisotropies

In this section, we want to discuss briefly the role of trap anisotropies in the creation of matter-wave bubbles. As the numerical simulations of the previous section have shown, bubbles can very well be manufactured in anisotropic traps if condensates of interacting atoms are used. However, it should be mentioned that in the absence of atomic interactions, the unavoidable trap anisotropies severely impede the bubble creation process. Imagine that in the bare magnetic trap $\omega_x=\beta\omega_z$, but we keep $\beta\approx1$. Then the effective trapping frequency along the x axis is given by $\beta\sqrt{\Delta/\Omega}$ (scaling now with respect to ω_z). We can model our system Hamiltonian as

$$H=-\frac{\nabla^2}{2}+\frac{1}{2}\omega_0^2(\theta)(r-r_0)^2, \quad (17)$$

where $\omega_0(\theta)$ appropriately interpolates between $\sqrt{\Delta/\Omega}$ and $\beta\sqrt{\Delta/\Omega}$. The ground state is approximated as

$$\overline{\psi}_{tr}=\frac{1}{\sqrt{\mathcal{N}}}\frac{\exp[-(r-r_0)^2/2\sigma(\theta)^2]}{r}\overline{f}(\cos\theta) \quad (18)$$

with $\sigma(\theta)=1/\sqrt{\omega_0(\theta)}$. We again could determine $\overline{f}(\cos\theta)$ by minimizing the energy functional. However, following the discussion of the previous paragraph we can argue that variations in the angular kinetic energy carry a cost of the order of $1/\Delta$ whereas the difference in ''polar potential energy'' is given by $|\beta^2-1|\Delta/\Omega$. Therefore, we expect trap anisotropies to have a significant influence as soon as

$$\left|\left(\frac{\omega_x}{\omega_z}\right)^2-1\right|\frac{\Delta}{\Omega}\gtrsim\frac{1}{\Delta}. \quad (19)$$

As typically $\Delta\gg1$ and $\Delta/\Omega\gg1$, the trap frequencies have to be adjusted very carefully in order to enable the generation of bubbles. In the case of Fig. 2, for example, the estimate (19) indicates that $|\omega_x/\omega_z-1|$ should be of the order of 0.1%. Fortunately, the problem can be alleviated to some

extent by making use of the atomic interactions. In the Thomas-Fermi limit, the chemical potential of a thin bubble is estimated to be

$$\mu = \left(\frac{3}{4\sqrt{2}} \frac{UN}{\sqrt{\Omega\Delta}} \right)^{2/3} \tag{20}$$

with $U = a_{scat}/a_{ho}$ as the scaled nonlinearity coefficient and where N is the number of atoms in the bubble. The chemical potential μ is measured with respect to the bottom of $V_+(r)$. We expect that only if the nonlinear interaction energy—which is of the order of μ—is in sufficient excess of the effective potential energy, i.e., if

$$N \gg \frac{4\sqrt{2}}{3U} |\beta^2 - 1|^{3/2} \frac{\Delta^2}{\Omega}, \tag{21}$$

then a bubble of approximately constant density can be formed. Thus, even if gravity is compensated for, bubbles can probably only be produced in the presence of strong nonlinear interactions. The numerical simulations of the previous section have shown that under such conditions a preparation may indeed be possible.

IV. APPLICATIONS OF BUBBLES

A. Production of excited harmonic-oscillator states

As a first application of matter-wave bubbles we now discuss the preparation of excited harmonic-oscillator states in the absence of nonlinear interactions (i.e., for sufficiently dilute samples). If, after creating a bubble state, the coupling strength is slowly *reduced at fixed* Δ the system will again evolve through a sequence of instantaneous eigenstates. This time, however, the eigenstate will not significantly change its energy relative to the minimum of the bare trapping potential. Qualitatively speaking, the wave function gradually moves out from the crossing region where it is being trapped and begins to experience more strongly the presence of the bare harmonic potential. This process is accompanied by a loss of atoms which end up on the repulsive potential after leaving the crossing region. At $\Omega = 0$ the remaining bound wave function will have reached an excited harmonic-oscillator eigenstate which, in the spherical harmonic case, is characterized by having $l = 0$. As mentioned before, the energy of this eigenstate is approximately equal to the energy of the initial bubble state. To give an example, if we start from the state shown in Fig. 1(b), and the coupling strength is ramped down within a time interval of $\Delta t = 16$, we arrive at an eigenstate of energy 35.5 with respect to the minimum of the harmonic potential [14]. A sequence of intermediate states appearing in the course of this process is shown in Fig. 4. After completion, the admixture of other eigenstates is less than 2%, and the population is 36% of the initial population in the harmonic trap ground state.

A few remarks should be made about this preparation scheme.

(i) It has to be performed ''quasiadiabatically,'' i.e., slow enough to avoid substantial excitation of other eigenstates, but sufficiently fast to reduce losses as much as possible.

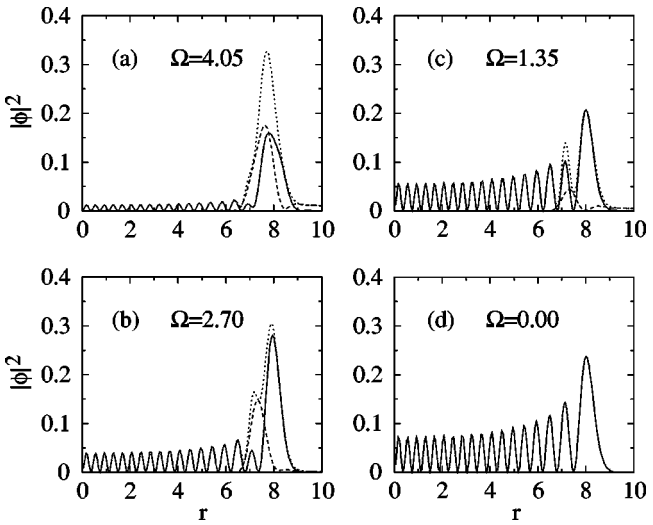

FIG. 4. Resonance states of Eqs. (6) at $\Delta = 60$ and various values of Ω (nonlinearities not taken into account). The wave functions are determined numerically by slowly decreasing the value of Ω in Eqs. (6) after initially preparing a bubble state. Full curves, $|\phi_1|^2$; dashed, $|\phi_2|^2$; dotted, sum of both. The displayed wave functions are normalized to one.

(ii) Although the system effectively ends up with the same Hamiltonian as in the very beginning (coupling switched off) and the time evolution is performed quasiadiabatically, the final state is very different from the initial one. This is because the Hamiltonian depends on two external parameters Ω and Δ, and $\Omega = 0$ represents a singularity in the sense that the value of Δ becomes irrelevant.

(iii) The oscillator eigenstates can in turn be used as intermediate states to produce radially excited bubble states. To this end, one simply switches the field coupling on again with a reduced detuning.

B. Nonlinear eigenstates

The bubble states can be regarded as the ground states of a specifically tailored potential. Recently, however, the study of macroscopically excited states of BECs has received much attention [20,21] and the manufacture of harmonic-oscillator eigenstates, as presented above, indicates a way to prepare a new class of such excited states. This class can be thought of as the nonlinear generalization of the eigenstates of linear systems; for a one-dimensional model some properties of such ''nonlinear modes'' were examined in Ref. [22] without discussing ways for their actual preparation. For highly excited states, nonlinear effects are expected to play a minor role, in general, because of the reduced density. We thus focus here on the first excited nonlinear $l = 0$ mode which is characterized by one radial node in the wave function. In the absence of nonlinear interactions the preparation scheme of Sec. IV A works equally well for low- and high-lying eigenstates, so we have numerically applied the same approach, with suitably chosen values for Ω and Δ, to the full Gross-Pitaevskii equation. Our studies show that the scheme is still applicable, though the atomic interactions cause detrimental effects: shortly before reaching the final

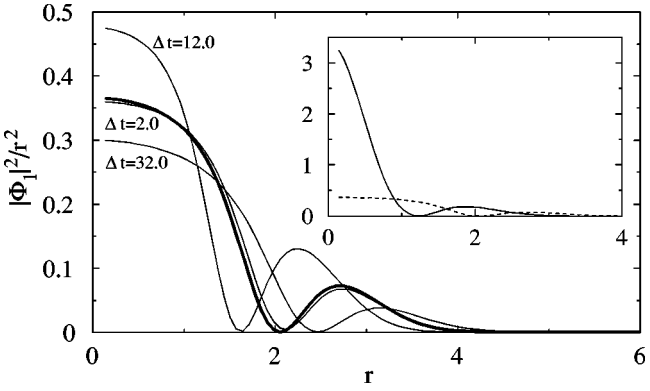

FIG. 5. Condensate density $|\phi_1|^2/r^2$ at times $\Delta t=2$, 12, and 32 after completion of the preparation scheme. Preparation proceeds from the bubble state at $\Omega=5.6$ and $\Delta=5.4$ by reducing Ω to 0 within $\Delta t=70$. The bold curve shows the exact "nonlinear mode" for the final value $NU_{11}=17.2$. The inset compares this state (dashed) to the corresponding eigenstate in the absence of nonlinearities (full curve).

value of $\Omega=0$ one encounters a very strong loss of atoms, and, because of this, the process has to be performed rather quickly resulting in an appreciable excitation of the final wave function. Furthermore, the final detuning Δ has to be selected more carefully (to within $\pm 0.1\omega$) to optimize the number of atoms that remain trapped. In spite of these difficulties, satisfactory results can be obtained for final nonlinearity parameters NU_{11} up to the order of 10. As an example, Fig. 5 shows the density distribution $|\phi_1(r)|^2/r^2$ at various instances after completion of the preparation process (for which $U_{11}=U_{22}=1.08U_{12}$ was assumed, as in ^{23}Na). The breathing seen in the wave function indicates that there is additional radial excitation. The parameter $NU_{11}=17.2$, and the projection onto the exact stationary state at this value varies between 60% and 95%. The efficiency, i.e., the ratio of final and initial atom number, is 9.5%. The comparison with the eigenstate of the linear case (see inset) shows a broadening of the wave function and a significant reduction of the central density due to the interatomic repulsion.

C. Collapse, revival, and free expansion

Another interesting effect occurs if, after creating the bubble, the coupling strength Ω is instantaneously reduced to zero. In this case, the two components of the bubble evolve almost independently of each other in their respective bare potentials. Component 2 is therefore rapidly expelled from the trapping region, whereas component 1 undergoes a collapse or contraction into the center of its binding harmonic potential followed by a reexpansion. If nonlinear interactions can be neglected this scenario repeats itself periodically, the wave function regaining its initial shape at times $n\pi$, $n=1,2,\ldots$. In the presence of atomic interactions, however, the shape is gradually distorted. Figure 6 shows $|\phi_1(r)|^2$ for three different values of gN at times $t=1.6$ and 3.2, i.e., for "complete" collapse and reexpansion, respectively. In the large figure the wave functions show an interference pattern which is due to particles from opposite sides of the bubble passing through each other. Note that for growing nonlinear interaction the central interference fringes are pushed outwards in agreement with earlier studies on similar systems (see, e.g., Ref. [23]). It might be possible to infer the nonlinearity parameter from the fringe pattern. The inset in Fig. 6 illustrates the subsequent broadening of the wave function in the course of the reexpansion due to nonlinear interactions.

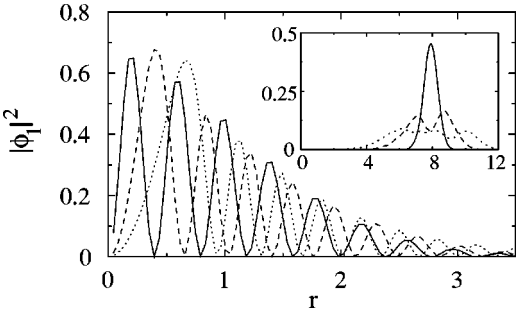

FIG. 6. Condensate density $|\phi_1|^2$ at times $\Delta t=1.6$ and 3.2 (inset) after suddenly switching off the rf coupling Ω. The different curves have nonlinearity parameters $UN=0$ (full curve), 5 (dashed), and 20 (dotted). In each case, the initial state was the respective matter-wave bubble at $\Delta=60$ and $\Omega=9$.

A related behavior can be observed if the magnetic fields are switched off along with the rf coupling. As it is no longer subject to any potential, the localized radial bubble wave function displays a time evolution similar to a free particle and gradually broadens due to dispersion (see Fig. 7). After some time wave-function pieces from opposite sides of the bubble start to overlap each other and an interference structure ensues. Again, the interference fringes are shifted outwards if nonlinear interactions become significant (see the inset).

V. DISK-SHAPED CONDENSATES

In this section we examine how our trapping scheme is modified in the presence of gravity and in the absence of any gravitational compensation (such as described in Sec. III D). The results will also lay the foundation for our proposal for

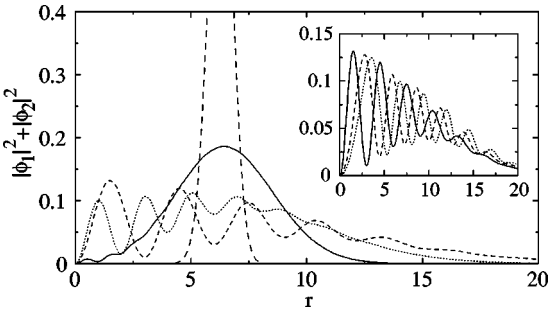

FIG. 7. Condensate density $|\phi_1|^2+|\phi_2|^2$ at times $\Delta t=0.0$ (long dashed), 2.0 (full), 4.0 (dotted), and 6.0 (short dashed) after suddenly switching off both the RF coupling and the magnetic potential. The initial state is the matter-wave bubble at $\Delta=40$, $\Omega=9$, and $UN=0$. In the inset the condensate density is shown at $\Delta t=6.0$ for nonlinearity parameters $UN=0$ (full curve), 20 (dashed), and 40 (dotted).

the creation of 2D atom traps which is outlined in the following Sec. VI.

A. Adiabatic trapping in the presence of gravity

To make the presentation more concrete, we look at a specific example that corresponds to typical experimental conditions. We thus consider a condensate of about 10^5 ^{87}Rb atoms initially prepared in the $F=2$, $M_F=2$ hyperfine sublevel and in the ground state of an anisotropic magnetic trap with frequencies $\nu_y=\nu_z=220$ Hz and $\nu_x=11$ Hz. The z axis again points along the vertical direction. A RF field is then applied that couples the sublevels within the $F=2$ multiplet. By appropriately tailoring the time dependence of the field, the BEC always remains in the ground state of the RF-induced adiabatic potential and is thus manipulated in a controlled way.

The condensate dynamics is determined by the Gross-Pitaevskii equation for the components ψ_M, M $=-2,\ldots,2$,

$$i\dot{\psi}_M=\left[-\frac{\nabla^2}{2}+\frac{M}{4}(\kappa^2x^2+y^2+z^2)-M\Delta(t)+Gz\right]\psi_M + \Omega_{M,M-1}(t)\psi_{M-1}+\Omega_{M+1,M}(t)\psi_{M+1} + UN\rho(r,t)\psi_M . \quad (22)$$

Again, all quantities are dimensionless. They are now scaled to units derived from the radial angular frequency $\omega_z=2\pi\nu_z$. The effective detuning is given by $\Delta(t)=[\hbar\omega_f-\Delta E(0)]/\hbar\omega_z$ with $\Delta E(0)$ the Zeeman energy split between subsequent hyperfine sublevels at the magnetic-field minimum. The parameter $\kappa=\nu_x/\nu_z$ gives the ratio between axial and radial trapping frequencies. The scaled gravitational acceleration G becomes 7.06 in the present setup. The rf coupling constants are given by $\Omega_{2,1}=\Omega_{-1,-2}=\sqrt{2/3}\Omega_{1,0}=\sqrt{2/3}\Omega_{0,-1}=\Omega(t)$. For simplicity, all nonlinear interaction coefficients are taken to be equal and denoted by U; N is the total number of atoms and $\rho(r,t)=\Sigma_{M=-2}^{2}|\psi_M(r,t)|^2$.

As discussed in Sec. III C, the simplified form of the nonlinear interaction allows us to transform to the dressed-eigenstate basis in the same way as in the linear case. The field-induced adiabatic potentials are now given by

$$\tilde{V}_M(\mathbf{r},t)=M\sqrt{[V_{tr}(\mathbf{r})-\Delta(t)]^2+\Omega^2(t)}, \quad (23)$$

where $V_{tr}(\mathbf{r})=(\kappa^2x^2+y^2+z^2)/4$, so that a wave packet initially prepared in the state $M=2$ can evolve in the potential $\tilde{V}_2(\mathbf{r},t)+Gz$ if the potential is deformed slowly enough. The approximate equation of motion for $\tilde{\psi}_2$ thus reads

$$i\dot{\tilde{\psi}}_2=\left[-\frac{\nabla^2}{2}+\tilde{V}_2(\mathbf{r},t)+Gz+UN|\tilde{\psi}_2(\mathbf{r},t)|^2\right]\tilde{\psi}_2 . \quad (24)$$

The influence of gravity becomes apparent by writing the z dependent part of the potential as $Mz^2/4+Gz=M(z+2G/M)^2/4-G^2/M$. We see that, effectively, the position of the bare trap minimum is shifted to $z=-2G/M$ (which typically is large compared to the ground-state extension), the minimum itself is shifted by $-G^2/M$. At $\Delta=0$ all bare potentials touch at $z=0$. The bare potential for $M=-2$ intersects the $M=2$ potential at its minimum for $\Delta=G^2/4$. As the condensate is initially localized at this minimum, we conclude that only for $\Delta\gtrsim G^2/4$ does a significant shift and deformation of the ground state set in. For large Δ the ground state is located at about $2\sqrt{\Delta}$. In Fig. 8 we show cuts along the potentials in the z direction that illustrate the characteristic behavior explained above.

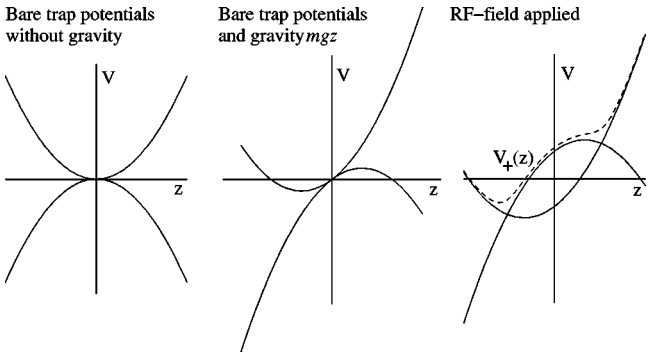

FIG. 8. Schematic of the potentials along the z direction showing the characteristic influences of gravity and the applied RF field.

What does the full spatial dependence of the potential $\tilde{V}_2(\mathbf{r},t)+Gz$ look like? The potential $\tilde{V}_2(\mathbf{r},t)$ alone has its minimum on an ellipsoidal surface defined by $V_{tr}(\mathbf{r})=\Delta(t)$. However, due to the influence of gravity the combined potential $\tilde{V}_2(\mathbf{r},t)+Gz$ is strongly tilted in the z direction, so that the wave function will assemble around its bottom (we will see this in Fig. 10). The main control parameter to vary the shape of the adiabatic potential is the detuning Δ. At a given Δ the coupling strength Ω has to be chosen large enough so that the lifetime of the condensate becomes sufficiently long.

B. Preparation

To demonstrate that atoms can be actually be trapped in the rf-induced adiabatic potential we have performed numerical simulations of Eq. (22) in two dimensions, i.e., the direction of gravity z and the weak trapping direction x. These calculations should be able to capture the main aspects of the wave-packet behavior. Our results indicate that the same two-step approach as outlined in Sec. III can be used to transfer the BEC into the adiabatic trap. As an illustration, we show in Fig. 9 the result of one of our simulations. For the 2D calculation, the nonlinearity parameter NU was chosen so that the extension of the ground state in the bare magnetic trap [which is the initial state $\psi_2(t=0)$] coincides with the extension in x and z of the 3D ground state for the given atom number of 10^5. In the first step of the preparation scheme, the rf intensity is linearly ramped up to the desired final value of Ω at *negative* Δ. In Fig. 9, in order to reach a final $\Omega=12$ (≈ 2.64 kHz) the field is switched on at $\Delta=-5(\approx -1.1$ kHz) within $\Delta t=20\simeq 14.4$ ms. In the second step the rf detuning is simply increased to the final value thereby keeping the intensity fixed. In Fig. 9, the detuning Δ

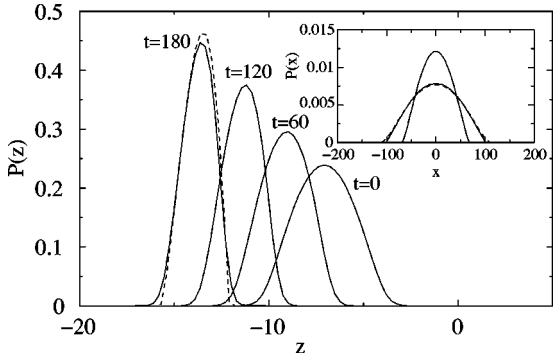

FIG. 9. Loading an adiabatic trap in the presence of gravity. Shown is the x-integrated density $P(z)=\int dx \Sigma_{M=-2}^{2}|\psi_M(x,z)|^2$ at the indicated times for the preparation process described in the text. The inset shows the z-integrated density $P(x)$ at $t=0$ and 180. The dashed curves show P as obtained from the Thomas-Fermi approximation.

was increased to 60($\approx$13.2 kHz) within $\Delta t=160\simeq 116$ ms. The simulations already show the deformation effect that we build upon in the following section to obtain 2D trapping, namely, a squeezing in the z direction indicating tighter trapping, and an expansion in x showing the decrease in the corresponding trap frequency. Furthermore, we see that the Thomas-Fermi approximation gives a very good description of the wave function. Nevertheless, it should be mentioned that during preparation a slight excitation of the wave function along the x axis appears (not visible in Fig. 9) indicating some nonadiabatic effects.

The effort required for the numerical calculations shows that it is very difficult to go significantly beyond the trap deformations shown in the above example—and in particular to simulate reaching the 2D limit. In the following section we give some semiquantitative arguments to determine the values of Ω and Δt that should be used to reach a given Δ. Here we restrict ourselves to a qualitative discussion. The chosen Δ places a lower limit on the value of Ω—only for a high enough Ω is the lifetime of the BEC in the adiabatic potential sufficiently long. For this complicated five-state system it is difficult to estimate the lifetimes analytically in an accurate way. However, the numerical calculations indicate that with, for example, $\Delta=60$, a value of $\Omega=12$ should be adequate. Furthermore, the study of the linear two-state system shows that the lifetime increases exponentially with Ω. We thus expect that the lifetime can always be adjusted by a moderate increase in Ω.

Concerning the rise times Δt, they are bounded from below by the requirement that we want to avoid nonadiabatic excitations and keep the BEC in the ground state. We expect that it is more likely we would generate such excitations along the x direction than along the radial directions as in the former the eigenstates are spaced much more closely. In fact, this is observed in the numerical simulations as mentioned above. The amount of excitation is reduced by performing the process more slowly. An upper limit on the rise time is placed by the lifetime of the adiabatic ground state and the overall decay time of the BEC.

C. Signatures of adiabatically trapped BECs

There are various signatures which allow one to verify experimentally that the condensate behavior is indeed determined by the adiabatic potential (apart from the fact that the BEC is still there at all):

(1) The vertical position of the condensate is changed (lowered). With $z=0$ indicating the minimum of the magnetic trap field the condensate is located around $z=-G$ (≈ -5.1 μm for our example) in the absence of the applied rf fields. With these fields turned on at sufficiently large Δ the potential minimum is shifted to the vicinity of the intersection between the different bare potentials at $x=y=0$, $z=-2\sqrt{\Delta}$. For $\Delta=60$, e.g., the condensate center is transferred to -11.3 μm, i.e., it is shifted over a distance larger than the BEC extension in the z direction.

(2) The shape of the condensate is changed. At $\Delta=40$, $\Omega=12$ the full width σ_z in z is about half the width of the rf-field-free case [24], whereas the width in x has increased by about 50%. This change of shape should influence the ballistic expansion of the BEC once the trapping fields are switched off. Furthermore, the condensate is slightly bent in the z direction.

(3) The ground state in the adiabatic potential is a dressed state, i.e., it is a superposition of different hyperfine sublevels. Observing the different hyperfine components would very convincingly demonstrate the trapping of the BEC in the adiabatic potential.

(4) If the rf fields are suddenly switched off the components $M_F=1$ and 2 should perform harmonic oscillations in their respective magnetic trapping potentials.

VI. TWO-DIMENSIONAL ATOM TRAPPING REGIME

A. Basic considerations for 2D atom traps and 2D BEC

Having introduced field-induced adiabatic potentials as a means to create new types of trapping potentials, we now turn to the question of how they can be used to obtain a two-dimensional atom trap by the appropriate choice of strong fields and large detunings. Unfortunately, as mentioned above, in these parameter regimes the resulting systems are hard to model numerically. So in this section we will use general arguments to show under what conditions it might be possible to obtain 2D trapping, and even a 2D BEC, using the kind of adiabatic loading scheme mentioned in Sec. V. These arguments will allow us to relax the restriction on the geometry of the system somewhat (the magnetic trap can now have three different frequencies). However, in our discussion we explicitly consider a two-state system (rather than general multilevel systems). Nevertheless we expect that much of the discussion of a two-state system would hold qualitatively for multilevel systems with an appropriate choice of parameters.

In general, a 3D harmonic potential with angular frequencies ω_1, ω_2, ω_{trans} provides an effective two-dimensional trap for atoms of temperature T, if

$$\hbar\omega_{1,2}<k_BT<\hbar\omega_{trans} \tag{25}$$

(from now on we return to unscaled quantities). Thus a good

2D trap has a large ω_{trans} to allow one motional degree of freedom to be frozen out at high temperatures. For an ideal gas, Bose condensation in a 2D harmonic trap occurs at

$$k_B T_c = \hbar \bar{\omega} \sqrt{6N/\pi} \tag{26}$$

with $\bar{\omega} = (\omega_1 \omega_2)^{1/2}$ and N the number of atoms [25]. Thus, combining Eqs. (25) and (26), the number of atoms that can undergo a genuine 2D condensation satisfies the condition $N \lesssim (\omega_{trans}/\bar{\omega})^2$. For a higher number of atoms condensation would have occurred already in the 3D regime. Therefore we see that, to aim for a 2D BEC, a high ratio $\omega_{trans}/\bar{\omega}$ is a further desirable criterion for a 2D trap, especially considering that small numbers of atoms would be hard to image experimentally.

B. Two-dimensional atom trapping and adiabatic potentials

We will generalize the discussion in Sec. V so that we now allow the original magnetic trap to have different oscillator frequencies ω_x, ω_y, and ω_z along the three axes with corresponding oscillator lengths a_x, a_y, a_z. (Note that $a_i = \sqrt{\hbar/m\omega_i}$, $i = x,y,z$.) Thus the corresponding magnetic trap has the potential

$$V_{tr}(\mathbf{r}) = \tfrac{1}{2} m(\omega_x^2 x^2 + \omega_y^2 y^2 + \omega_z^2 z^2), \tag{27}$$

where, again, we are now working with unscaled quantities. As in Sec. III, we consider a two-level system and assume that the second state experiences the magnetic potential $-V_{tr}$.

The upper field-induced adiabatic potential, which is the potential of greatest interest, is then given by

$$\tilde{V}(\mathbf{r},t) = mgz + \tilde{V}_+(\mathbf{r},t) \tag{28}$$

with

$$\tilde{V}_+(\mathbf{r},t) = \sqrt{[V_{tr}(\mathbf{r}) - \hbar\bar{\Delta}(t)/2]^2 + [\hbar\Omega(t)]^2}. \tag{29}$$

Here $\bar{\Delta}$ denotes the unscaled detuning, i.e., $\bar{\Delta} = \omega_f - \Delta E(0)/\hbar$ with ω_f the rf-field frequency and $\Delta E(0)$ the minimum energy difference between the hyperfine states (see Sec. II A). The bare potentials intersect, where there is resonance, i.e., at the locations $\hbar\bar{\Delta}(t) = 2V_{tr}(\mathbf{r})$. This intersection we call the ''seam'' of the bare potentials. In the absence of gravity, the seam of $\tilde{V}_+$ would also be the location of the minimum in $\tilde{V}$ and would have the shape of an ellipsoid with radii $r_i = (\bar{\Delta}/\omega_i)^{1/2} a_i$, $i = x,y,z$. Thus, without gravity, or gravity being compensated for, the atom distribution forms an ellipsoid bubble, or shell in the potential (29).

Under the influence of gravity the atoms sag to the bottom of the shell potential (28), and this would not allow the formation of a matter-wave bubble. In fact, as shown in Sec. III D, a closed bubble could exist only up to radii $r \lesssim (\hbar^2/gm^2)^{1/3}$ ($\simeq 5\times10^{-7}$ m for ^{87}Rb). Under typical experimental conditions we can expect a situation as depicted in Fig. 10 which shows—for the indicated parameter values—the potential $\tilde{V}$ in the plane $y=0$ along with an atomic BEC in the ground state for this potential.

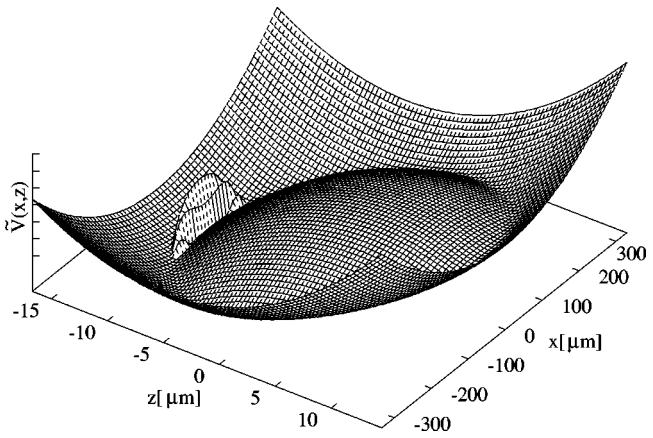

FIG. 10. Adiabatic potential $\tilde{V}(\mathbf{r}) = \tilde{V}_+(\mathbf{r}) + mgz$ (in arbitrary units) at $y=0$ for $\omega_x/2\pi = 11$ Hz, $\omega_y/2\pi = \omega_z/2\pi = 220$ Hz, $\bar{\Omega}/2\pi = 2.6$ kHz, and $\bar{\Delta}/2\pi = 66$ kHz. Inserted is the ground state of a ^{87}Rb condensate with about 10^5 atoms.

Typically, an atom moving in the potential $\tilde{V}$ is confined to the close proximity of the seam due to the strong confinement in the direction transverse to it. If its energy E satisfies $E \ll mgr_z$, it is also restricted to the vicinity of the bottom of $\tilde{V}$ because of gravity. To a good degree of approximation the atomic motion can therefore be modeled as harmonic. To determine the harmonic frequencies we can expand Eq. (28) about $z = -r_z$ to find

$$\omega_{1,2} = (g/r_z)^{1/2} \omega_{x,y}/\omega_z \tag{30}$$

along the surface of the seam, and

$$\omega_{trans} = (\bar{\Delta}/\bar{\Omega})^{1/2} \omega_z \tag{31}$$

in the normal direction. Here the unscaled coupling frequency is denoted by $\bar{\Omega}$. The oscillator lengths corresponding to $\omega_{1,2}$ and ω_{trans} will be denoted by a_{trans}, a_1, and a_2. The effect of gravity on the potential will also shift it downwards so that the equilibrium point is now at

$$z_0 \sim -\sqrt{\frac{\hbar\bar{\Delta}}{m\omega_z^2}} - \frac{g}{\omega_{trans}^2}. \tag{32}$$

However, the displacement of g/ω_{trans}^2 is rather small and also turns out not to be sufficient to violate the harmonic expansion of Eq. (28) which results in Eqs. (30) and (31). (See Sec. VI C 3 below.)

C. Conditions for 2D trapping in adiabatic potentials

The obvious strategy for realizing a 2D trap is to increase the detuning $\bar{\Delta}$ as much as possible in order to obtain strong radial confinement. A sufficiently large coupling $\bar{\Omega}$ will be necessary to ensure that the potentials remain adiabatic. To arrive at a 2D trap, a number of considerations have to be taken into account (some given previously in Ref. [9]), and

these factors determine how large $\overline{\Omega}$ and $\overline{\Delta}$ need to be, and the relationship between them.

1. Lifetime

For a given $\overline{\Delta}$, the rf coupling strength $\overline{\Omega}$ has to be chosen accordingly to ensure a sufficiently large lifetime for atoms held in the adiabatic trap. Equation (10) gives an estimate of the decay rate and if we require that the decay rate is less than a certain maximum, i.e.,

$$\gamma_{ex} \leqslant \gamma_{max}, \tag{33}$$

it follows from Eq. (10), when unscaled, that one needs

$$\overline{\Omega}^3 \geqslant \lambda \omega_z^2 \overline{\Delta} \tag{34}$$

with the parameter $\lambda = 2[\ln(\gamma_{max}/2\omega_z)]^2/\pi^2$. Thus the worst allowed decay rate can be specified in terms of the vertical trap frequency. In the numerical example below (Sec. VI D) we choose $\gamma_{max}/\omega_z = 0.01$ so that $\lambda = 5.7$.

As indicated in Sec. V B, analytical expressions for the lifetime in general multistate systems are not available. However, we expect that our estimates are still valid, at least as a first approximation, under such conditions. This view is supported by our numerical study of the five-state system.

2. Strong binding and spatial thinness

The lifetime sets a lower limit on Ω at a given Δ. Choosing Ω too large, however, impairs the strong radial confinement. An upper limit is imposed by the obvious conditions

$$\omega_{trans} \gg \omega_{1,2} \tag{35}$$

and

$$r_z \gg a_{trans}. \tag{36}$$

The first of these was discussed in Sec. VI A and ensures that one spatial direction is effectively frozen out at low temperatures. The second condition guarantees that the atoms are tightly confined to the vicinity of the seam. Both these requirements are typically not in conflict with condition (34). Formally, this can be seen from the fact that the first condition translates into

$$\overline{\Omega}^2 \ll \frac{\overline{\Delta}^3 \omega_z^5 a_z^2}{g^2 \omega_{x,y}^4}, \tag{37}$$

where for $\omega_{x,y}$ one should choose the maximum of ω_x and ω_y to make the condition most restrictive. The second condition leads to

$$\overline{\Omega} \ll 4\overline{\Delta}^3/\omega_z^2. \tag{38}$$

Inequality (34) will allow us to choose $\overline{\Omega} \propto \overline{\Delta}^{1/3}$, so that the above conditions are increasingly easy to meet for growing $\overline{\Delta}$, in accordance with our expectation.

3. Harmonic 2D trapping

In this section we will look at the conditions for harmonicity of the trap. Harmonicity is probably desirable, but is not actually *essential* for trapping. The conditions derived below will show that the trap is operated in a 2D harmonic regime.

To be able to speak of a *harmonic* 2D trap at a finite temperature, one has to require that

$$\hbar \omega_{1,2} \ll k_B T_c \ll m g r_z. \tag{39}$$

The first criterion ensures that, at the condensation point, the atoms can reach sufficiently many quantum states to actually experience the trapping potential as being harmonic. It is automatically fulfilled if we substitute for T_c from Eq. (26) to find

$$N \gg \frac{\pi^2}{6}\left(\frac{\omega_{1,2}}{\omega_{2,1}}\right), \tag{40}$$

where from Eq. (30) $\omega_{1,2}/\omega_{2,1} = \omega_{x,y}/\omega_{y,x}$ is the ratio of trapping frequencies in the x-y plane. Equation (40) should be easily satisfied if there are to be any significant number of atoms in the trap.

The second part of Eq. (39) leads to

$$k_B T_c \ll \frac{g\overline{\Delta}^{1/2}}{a_z \omega_z^{5/2}} \tag{41}$$

when we substitute for r_z. This second criterion makes sure that anharmonic effects in the trapping potential can be neglected. The same condition arises as the condition for harmonic motion of a single particle confined to the seam. (A picture which assumes tight transverse trapping.) In the example below $mgr_z/k_B \simeq 18\ \mu$K which is much larger than $T_c \simeq 0.3\ \mu$K. Note, however, that the appearance of anharmonic effects in the 2D trapping potential does not automatically affect the two-dimensionality of the trap.

We can also ask if we have harmonicity in the third, transverse, direction. If we focus on the bottom of the potential, i.e., take $x = y = 0$, the adiabatic potential (28) simplifies to

$$\tilde{V}(z,t) = mgz + \sqrt{[m\omega_z^2 z^2/2 - \hbar\overline{\Delta}(t)/2]^2 + [\hbar\Omega(t)]^2}. \tag{42}$$

Then in an adiabatic regime, one limit which produces quite simply a harmonic potential is found from the condition

$$\hbar\Omega(t) \gg \left|\frac{1}{2}m\omega_z^2 z^2 - \hbar\overline{\Delta}(t)/2\right|, \tag{43}$$

which, together with

$$|z - z_0|/|z_0| \ll 1, \tag{44}$$

allows a quadratic expansion of Eq. (42). An estimate for z_0, the location of the minimum, has been given in Eq. (32). At $z = z_0$ we may substitute Eq. (32) into Eq. (43) to eventually obtain

$$\overline{\Delta} \gg \frac{g^2}{a_z^2 \omega_z^3}. \tag{45}$$

Here we also assumed that the shift of z_0 away from $-r_z = -\sqrt{\hbar\overline{\Delta}/m\omega_z^2}$ [see Eq. (32)] was very small so that the smallest term could be dropped from z_0^2. The condition for this approximation is that

$$\sqrt{\frac{\hbar\overline{\Delta}}{m\omega_z^2}} \gg \frac{g}{\omega_{trans}^2} \tag{46}$$

which would lead to the subsidiary condition

$$\overline{\Delta}^3 \gg \frac{g^2\overline{\Omega}^2}{a_z^2\omega_z^3}, \tag{47}$$

when we substitute for ω_{trans}.

In considering values of z away from z_0 in Eqs. (44) and (43), we need an estimate of the thickness of the matter-wave disk. A distance characterizing this could be a_{trans}, i.e., we would use a single-particle wave-function width as a measure of the size of $|z-z_0|$ in Eq. (44). This equation is then already satisfied by Eq. (36) and the remaining condition Eq. (43) is also, approximately, satisfied if we accept the scaling of Eq. (34) (with a typical value of λ).

It turns out that it is possible to satisfy all the constraints in this section. It is even the case that violation of Eqs. (40) and (41) need not prevent a 2D BEC since there is no reason why a BEC cannot be 2D in an anharmonic regime; Eq. (26) would simply not apply. Likewise, anharmonicity in the transverse direction, resulting in violation of conditions (45) and (47) need not prevent 2D trapping or a 2D BEC.

4. Loading

A straightforward way to load the 2D trap consists in starting from a condensate in the original magnetic potential and then adiabatically transferring it to the 2D trap by appropriately switching on the rf field. The minimum duration of this process can be estimated by stipulating the adiabaticity condition $\dot{\omega}_{1,2} \ll \omega_{1,2}^2$. Using relation (34) this leads to

$$t \gg \frac{1}{\omega_{1,2}} = \frac{(\overline{\Omega}/\omega_{x,y})^{3/4}}{\lambda^{1/4}\sqrt{g/a_{x,y}}}. \tag{48}$$

Note that during loading, $\overline{\Omega}$ can be increased above the intended final value to reduce intermediate adiabatic losses.

5. Temperature

For the trap to be 2D at a temperature T the second part of Eq. (25) applies ($k_BT < \hbar\omega_{trans}$) which with the substitution of Eq. (31) leads to

$$k_BT \ll \sqrt{\frac{\overline{\Delta}}{=}}\hbar\omega_z. \tag{49}$$

If we take the case of equality in Eq. (34) and substitute for $\overline{\Delta}$ we find

$$k_BT \ll \hbar\overline{\Omega}/\sqrt{\lambda}. \tag{50}$$

We would expect this condition to be more restrictive than Eq. (41) which leads to $k_BT \ll \hbar\overline{\Omega}^{3/2}g/2\sqrt{\lambda}a_z\omega_z^{7/2}$. Thus, by substituting Eq. (26) into Eq. (50), the number of atoms that can undergo a 2D condensation is limited by

$$N \ll \frac{\pi^2\overline{\Omega}^2}{6\lambda\overline{\omega}^2}. \tag{51}$$

If we now utilize $\overline{\omega} = (\omega_1\omega_2)^{1/2}$ and Eq. (30) we finally obtain

$$N \ll \frac{\pi^2 a_z \overline{\Omega}^{7/2}\omega_z^{1/2}}{6g\lambda^{3/2}\omega_x\omega_y}. \tag{52}$$

Since Eq. (52) puts an upper bound on the number of atoms it is desirable to have as large a coupling $\overline{\Omega}$ as possible.

In fact none of the conditions above constrain $\overline{\Omega}$ if the connection (34) is accepted. The higher the value of $\overline{\Omega}$ the better [as in Eq. (52)]. However, from a practical point of view, it would be desirable to find the lowest viable $\overline{\Omega}$. This is determined by the most restrictive inequality on $\overline{\Omega}$. That is, if we place each of our various inequalities in the form $\overline{\Omega} > k$, where k contains the remaining constants, we will look for the inequality with the largest constant k. For realistic values of λ and $\omega_{x,y}$ this appears to be Eq. (45), which on substitution of Eq. (34) leads to

$$\overline{\Omega}^7 \gg \lambda^3 g^2 \omega_z^3/a_z^2. \tag{53}$$

Any value of $\overline{\Omega}$ greater than this would be suitable, but note that increasing $\overline{\Omega}$ also increases the loading time, Eq. (48), and this is ultimately undesirable. To see what is realistically possible we must now determine some values for a practical case.

D. Numerical estimate

We reported a numerical estimate in Ref. [9], where we considered a typical Ioffe-Pritchard trap with $\omega_x/2\pi = 11$ Hz, $\omega_y/2\pi = \omega_z/2\pi = 220$ Hz containing ^{87}Rb atoms initially in the $F=2$, $M=2$ ground state. In order to match approximately the two-state theory given above to this five-state system we need to replace $\overline{\Delta}$ by $4\overline{\Delta}$ to obtain the correct condition for resonance. The trap potential (27) becomes that for the $M_F=2$ state, and the coupling $\overline{\Omega}$ is replaced by $2\overline{\Omega}$. Then an rf field with a final coupling $\overline{\Omega}/2\pi = 15$ kHz and [from Eq. (34)] $\overline{\Delta}/2\pi = 12.2$ MHz is one that can be provided with currently available technology [26]. The condition (53) is easily satisfied since it results in $\overline{\Omega}/2\pi \gg 405$ Hz. The resulting trap frequencies are $\omega_{trans}/2\pi = 8.9$ kHz, $\omega_1/2\pi = 1.3$ Hz, $\omega_2/2\pi = 27$ Hz. The new trap is

vertically shifted by 0.34 mm from the center of the original magnetic potential. The critical temperature is given by 0.43 μK, so that up to 3.6×10^6 atoms could be condensed. The transverse width of the condensate is estimated at 0.08 μm if atomic interactions can be neglected. The time required for the preparation process should be large compared to $1/\omega_1$, Eq. (48), i.e., of the order of several seconds. In view of these estimates, the experimental realization of this new kind of 2D trap seems to be within reach of current experiments.

VII. SUMMARY AND CONCLUSIONS

In this paper we have shown that field-induced adiabatic potentials can provide a robust and versatile tool to create trapping configurations for ultracold atoms. As specific examples, we have considered the generation of matter-wave shell, or bubble, states and the preparation of two-dimensional atom traps. In a bubble state, the matter-wave density is localized around the surface of a three-dimensional sphere. We have discussed the preparation process which proceeds by coupling a harmonic magnetic trap to a repulsive harmonic potential by a suitably chosen time-dependent rf field. Although this configuration appears to be unstable at first sight, the bubbles are stabilized in the resulting dressed potential and their lifetime increases exponentially with the rf coupling strength. The bubbles can be used as stepping stones for the creation of highly excited oscillator eigenstates and ''nonlinear eigenmodes.'' We also investigated possible experiments showing collapse and revival effects. Although the creation of the bubbles is impeded by the influence of gravity and trap anisotropies, we have pointed out ways to overcome these difficulties with the help of present-day technology.

The same principle, which has been used for making bubble states, can also be applied to the creation of two-dimensional atom traps [27]. Under the combined influence of the dressing rf field and gravity, a condensate pools at the bottom of the resulting potential. By increasing the RF detuning the radial confinement becomes steeper, and the condensate gets increasingly squeezed until it eventually reaches a ''quasi-two-dimensional'' state. We have given estimates for the parameters necessary to reach this regime.

We hope that the results presented in this article stimulate further research into the possibilities that field-induced adiabatic potentials offer for the creation of new kinds of trapping potentials and lower-dimensional geometries. We have focussed in this paper on shell-like and disk-shaped traps, but by working with atomic waveguides we also expect that new tubular potentials could be formed. These new kinds of potentials can all be used to create new quantum-mechanical states of matter, and might also be used in the study of weakly bound clusters or nanoparticles.

ACKNOWLEDGMENTS

This work was supported by the United Kingdom Engineering and Physical Sciences Research Council. We would like to thank M. Boshier, C. Eberlein, and E. Hinds for discussions and comments.

APPENDIX

In this Appendix, we outline the derivation of Eq. (8) for the lifetime of the bubble states. The method is described in detail in Ref. [15] (see also Ref. [16]) so we can restrict ourselves to indicating the main steps.

Consider the time-independent linear version of Eq. (6),

$$\varepsilon\phi_1=\left(-\frac{1}{2}\frac{\partial^2}{\partial r^2}+\frac{r^2}{2}-\frac{\Delta}{2}\right)\phi_1+\Omega\phi_2,$$

$$\varepsilon\phi_2=\left(-\frac{1}{2}\frac{\partial^2}{\partial r^2}-\frac{r^2}{2}+\frac{\Delta}{2}\right)\phi_2+\Omega\phi_1 \tag{A1}$$

with ε the eigenenergy. We are interested in the structure of the solutions at energies $\varepsilon>\Omega$ for which resonance states are expected to appear. Far away from the potential crossing at $r_c=\sqrt{\Delta}$ the eigenfunctions $\phi_{1,2}$ can be approximated as [cf. Eq. (9) of Ref. [15]]

$$\phi_1(r\ll\sqrt{\Delta})\sim k_1^{-1/2}\left[A_1(\infty)\exp\left(i\int_{r_1}^{r}k_1dr+i\pi/4\right)+A_1(-\infty)\exp\left(-i\int_{r_1}^{r}k_1dr-i\pi/4\right)\right],$$

$$\phi_2(r\gg\sqrt{\Delta})\sim k_2^{-1/2}\left[A_2(\infty)\exp\left(i\int_{r_2}^{r}k_2dr-i\pi/4\right)+A_2(-\infty)\exp\left(-i\int_{r_1}^{r}k_1dr-i\pi/4\right)\right] \tag{A2}$$

with the classical momenta $k_1=(2\varepsilon-r^2+\Delta)^{1/2}$, $k_2=(2\varepsilon+r^2-\Delta)^{1/2}$ and the turning points $r_1=\sqrt{\Delta+2\varepsilon}$, $r_2=\sqrt{\Delta-2\varepsilon}$ (or $r_2=0$ if $\varepsilon>\Delta/2$). If we set, e.g., $A_2(-\infty)$ equal to unity then the other coefficients $A_i(\pm\infty)$ can be regarded as scattering amplitudes for the interaction process inside the curve-crossing region. Resonance states are related to poles of the scattering amplitudes in the complex energy plane. The determination of the amplitudes proceeds in two steps.

(i) By Taylor expanding the harmonic potentials to first order around the crossing at $r=r_c$, the interaction between the states 1 and 2 is described as a linear curve-crossing problem. Using the corresponding scattering matrix the amplitudes $A_1(\infty)$ and $A_2(\infty)$ can be expressed as linear functions of $A_1(-\infty)$ and $A_2(-\infty)$. The explicit formulas [Eq. (19) of Ref. [15]] involve the quantities δ and Φ introduced in Sec. III B. Note that the analytic form of the scattering matrix is only known approximately (see, e.g., Sec. IV of Ref. [17] for a comparison of different results), so that quantitative calculations based on the analytic approach depend somewhat on the expressions used.

(ii) The wave function ϕ_1 has to be subjected to appropriate boundary conditions, i.e., $\phi_1(r=0)=0$. This immediately yields the relation

$$A_1(\infty)/A_1(-\infty) = -\exp[2i\beta(\varepsilon)], \tag{A3}$$

where $\beta(\varepsilon)=\int_0^{r_1} k_1(r)dr - \pi/4 = \pi(2\varepsilon+\Delta-1)/4$.

Combining the results of (i) and (ii) and setting $A_2(-\infty)=1$ we finally obtain [cf. Eq. (29) of Ref. [15], note the sign error]

$$A_2(\infty) = \frac{\cos\beta(E)+[e^{2\pi\delta(E)}-1]\cos\Phi(E)e^{i[\beta(E)-\Phi(E)]}}{\cos\beta(E)+[e^{2\pi\delta(E)}-1]\cos\Phi(E)e^{-i[\beta(E)-\Phi(E)]}}. \tag{A4}$$

The poles of $A_2(\infty)$ are determined by condition (8).

[1] W. Ketterle, D.S. Durfee, and D.M. Stamper-Kurn, in *Bose-Einstein Condensation in Atomic Gases*, Proceedings of the International School of Physics ''Enrico Fermi,'' Course CXL, edited by M. Inguscio, S. Stringari, and C. Wieman (IOS Press, Amsterdam, 1999); e-print cond-mat/9904034.

[2] S. Heinrichs and W.J. Mullin, J. Low Temp. Phys. **113**, 231 (1998); T.L. Ho and M. Ma, *ibid.* **115**, 61 (1999); D.S. Petrov, M. Holzmann, and G.V. Shlyapnikov, Phys. Rev. Lett. **84**, 2551 (2000); M.D. Lee, S.A. Morgan, M.J. Davis, and K. Burnett, Phys. Rev. A **65**, 043617 (2002).

[3] M. Olshanii, Phys. Rev. Lett. **81**, 938 (1998); M.D. Girardeau and E.M. Wright, *ibid.* **84**, 5239 (2000); D.S. Petrov, G.V. Shlyapnikov, and J.T.M. Walraven, *ibid.* **85**, 3745 (2000).

[4] A. Görlitz, J.M. Vogels, A.E. Leanhardt, C. Raman, T.L. Gustavson, J.R. Abo-Shaeer, A.P. Chikkatur, S. Gupta, S. Inouye, T. Rosenband, and W. Ketterle, Phys. Rev. Lett. **87**, 130402 (2001).

[5] S. Burger, F.S. Cataliotti, C. Fort, P. Maddaloni, F. Minardi, and M. Inguscio, Europhys. Lett. **57**, 1 (2002).

[6] O. Morsch, M. Cristiani, J.H. Müller, D. Ciampini, and E. Arimondo, Phys. Rev. A **66**, 021601 (2002).

[7] W.L. Power, T. Pfau, and M. Wilkens, Opt. Commun. **143**, 125 (1997); H. Engler, I. Manek, U. Moslener, M. Nill, Y.B. Ovchinnikov, U. Schlöder, U. Schünemann, M. Zielonkowski, M. Weidemüller, and R. Grimm, Appl. Phys. B: Lasers Opt. **67**, 709 (1998); A.V. Taichenachev, A.M. Tumaikin, and V.I. Yudin, J. Opt. B: Quantum Semiclassical Opt. **1**, 557 (1999).

[8] E.A. Hinds, M.G. Boshier, and I.G. Hughes, Phys. Rev. Lett. **80**, 645 (1998).

[9] O. Zobay and B.M. Garraway, Phys. Rev. Lett. **86**, 1195 (2001).

[10] I. Bloch, M. Köhl, M. Greiner, T.W. Hänsch, and T. Esslinger, Phys. Rev. Lett. **87**, 030401 (2001).

[11] R.D. Levine, B.R. Johnson, and R.B. Bernstein, J. Chem. Phys. **50**, 1694 (1969).

[12] It should be noted that although the magnitude of V_c is reduced for growing Ω, the effective interaction range $\Delta r \simeq \Omega/C$ is increased. However, the size of the ground state of V_+ scales with $\Omega^{1/4}$, i.e., it only experiences the diminished magnitude of V_c.

[13] See, e.g., D.S. Hall, M.R. Matthews, J.R. Ensher, C.E. Wieman, and E.A. Cornell, Phys. Rev. Lett. **81**, 1539 (1998); M.R. Matthews, B.P. Anderson, P.C. Haljan, D.S. Hall, M.J. Holland, J.E. Williams, C.E. Wieman, and E.A. Cornell, *ibid.* **83**, 3358 (1999).

[14] O. Zobay and B.M. Garraway, Acta Phys. Slov. **50**, 359 (2000).

[15] M.S. Child, Mol. Phys. **16**, 313 (1969).

[16] M.S. Child, *Molecular Collision Theory* (Academic, London, 1974).

[17] C. Zhu and H. Nakamura, J. Chem. Phys. **98**, 6208 (1993).

[18] B.M. Garraway and K.-A. Suominen, Phys. Rev. Lett. **80**, 932 (1998); M. Rodriguez, K.-A. Suominen, and B.M. Garraway, Phys. Rev. A **62**, 053413 (2000).

[19] In fact, we utilize the two-dimensional version of Eq. (24) to which the optical potential (16) is added.

[20] M.R. Matthews, B.P. Anderson, P.C. Haljan, D.S. Hall, C.E. Wieman, and E.A. Cornell, Phys. Rev. Lett. **83**, 2498 (1999); K.W. Madison, F. Chevy, W. Wohlleben, and J. Dalibard, *ibid.* **84**, 806 (2000); S. Burger, K. Bongs, S. Dettmer, W. Ertmer, K. Sengstock, A. Sanpera, G.V. Shlyapnikov, and M. Lewenstein, *ibid.* **83**, 5198 (1999); J. Denschlag, J.E. Simsarian, D.L. Feder, C.W. Clark, L.A. Collins, J. Cubizolles, L. Deng, E.W. Hagley, K. Helmerson, W.P. Reinhardt, S.L. Rolston, B.I. Schneider, and W.D. Phillips, Science **287**, 97 (2000).

[21] P.O. Fedichev, A.E. Muryshev, and G.V. Shlyapnikov, Phys. Rev. A **60**, 3220 (1999).

[22] Y.S. Kivshar, T. Alexander, and S.K. Turitsyn, Phys. Lett. A **278**, 225 (2001).

[23] Wu-Ming Liu, Biao Wu, and Qian Niu, Phys. Rev. Lett. **84**, 2294 (2000).

[24] A rough estimate for σ_z can be obtained by expanding the adiabatic potential around its minimum and then applying the Thomas-Fermi approximation. Thereby, one obtains $\sigma_z \approx \sqrt{\tilde{\mu}\Omega/\Delta}$ with $\tilde{\mu}$ the new chemical potential (with respect to the potential minimum), which is typically somewhat higher than the original μ_0 ($\simeq 6.17\hbar\omega_z$ in the present case).

[25] V. Bagnato and D. Kleppner, Phys. Rev. A **44**, 7439 (1991).

[26] M.G. Boshier (private communication).

[27] Since submitting this paper we have found that two-dimensional atom trapping using the techniques of Sec. V has been achieved experimentally: Yves Colombe, Hélène Perrin, Brigitte Mercier, Elena Knyazchyan and Vincent Lorent (private communication).